Modeling Elastic Properties in Finite-Element Analysis: How Much Precision Is Needed to Produce an Accurate Model?

DAVID S. STRAIT,[1]* QIAN WANG,[2] PAUL C. DECHOW,[2] CALLUM F. ROSS,[3] BRIAN G. RICHMOND,[4] MARK A. SPENCER,[5] AND BIREN A. PATEL[6]

[1]Department of Anthropology, University at Albany, Albany, New York
[2]Department of Biomedical Sciences, Baylor College of Dentistry, Texas A&M Health Science Center, Dallas, Texas
[3]Department of Organismal Biology and Anatomy, University of Chicago, Chicago, Illinois
[4]Center for the Advanced Study of Hominid Paleobiology, Department of Anthropology, George Washington University, Washington, District of Columbia
[5]Department of Anthropology, Institute of Human Origins, Arizona State University, Tempe, Arizona
[6]Interdepartmental Doctoral Program in Anthropological Sciences, Stony Brook University, Stony Brook, New York

ABSTRACT

The influence of elastic properties on finite-element analysis was investigated using a finite-element model of a *Macaca fascicularis* skull. Four finite-element analyses were performed in which the model was assigned different sets of elastic properties. In analysis 1, elastic properties were modeled isotropically using published data obtained from human limb bones. Analyses 2–4 used data obtained from skulls of a closely allied species, *M. mulatta*, but varied as to how those data were incorporated into the model. In analysis 2, the model was assigned a single set of isotropic elastic properties. In analysis 3, each region within the model was assigned its own set of isotropic elastic properties. Finally, in analysis 4, each region received its own set of orthotropic elastic properties. Although a qualitative assessment indicates that the locations of strain concentrations across the model are broadly similar in all analyses, a quantitative assessment of strain indicates some differences between the analyses. When strain data from the finite-element analyses were compared to strain data derived from in vivo experiments, it was found that the model deformed most realistically using the orthotropic elastic properties employed in analysis 4. Results suggest that finite-element analyses can be adversely affected when elastic properties are modeled imprecisely, and that modelers should attempt to obtain elastic properties data about the species and skeletal elements that are the subjects of their analyses.

Key words: finite-element analysis; elastic properties; mastication

Hypotheses about the evolution of the primate masticatory system can be tested in part through an examination of bone strain in the primate facial skeleton (Hylander, 1984, 1986; Hylander et al., 1991; Ross and Hylander, 1996; Hylander and Johnson, 1997; Ross, 2001). Experimental studies of in vivo bone strain provide direct information about stress resistance in the facial skeleton, but for practical reasons, such information can only be obtained from a limited number of locations on the face. A valuable supplement to experimental studies is finite-element analysis (FEA), a standard engineering technique used to examine how objects of complex design resist load (Huiskes and Chao, 1983; Cook et al., 1989; Gross et al.,

*Correspondence to: David S. Strait, Department of Anthropology, University at Albany, 1400 Washington Avenue, Albany, NY 12222. Fax: 518-442-5710. E-mail: dstrait@albany.edu

Received 12 January 2005; Accepted 13 January 2005
DOI 10.1002/ar.a.20172
Published online 3 March 2005 in Wiley InterScience (www.interscience.wiley.com).

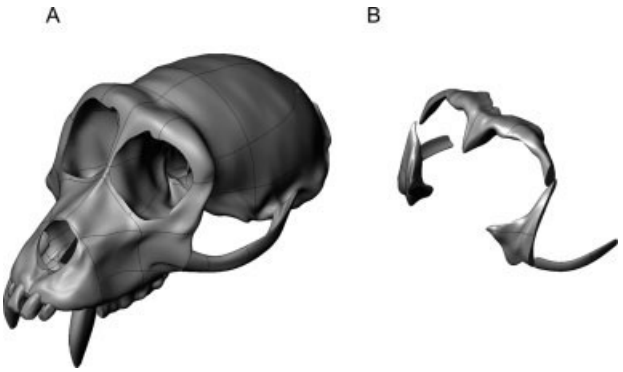

Fig. 1. Solid model of *M. fascicularis* skull. **A:** Parts of skull representing cortical bone. **B:** Parts of skull representing trabecular bone in the supraorbital torus, postorbital bar, zygomatic body, and zygomatic arch.

1992). Unlike strain gauge studies, FEA provides information about strain across an entire structure and therefore provides a global context in which to interpret experimental data.

FEA is a modeling technique and, like all such methods, is only as realistic as the variables on which the model is based. With respect to facial bone strain, key variables include the geometry of the facial skeleton, the elastic properties of facial bone, the forces produced by the muscles of mastication, and the manner in which the face is attached to, or constrained by, other parts of the skull. Advances in medical imaging techniques have made it possible to produce remarkably precise finite-element models of vertebrate skulls, but relatively less attention has been paid to variables other than geometry. This study examines the effect that elastic properties can have on finite-element analysis. A modeling experiment is performed in which a finite-element model of a macaque skull is analyzed multiple times while varying only the elastic properties assigned to it, thereby isolating the effect of this variable. Results of these analyses are compared to experimentally derived in vivo bone strain data so as to determine whether or not the deformations recorded in those analyses are realistic.

MATERIALS AND METHODS

Solid Model Creation

The finite-element model was based on the skull of a male *Macaca fascicularis* specimen housed at the National Museum of Natural History. *Macaca fascicularis* was chosen because this species has been the subject of prior studies of masticatory bone strain (Hylander, 1984; Hylander et al., 1991; Borrazzo et al., 1994; Hylander and Johnson, 1997). Sixty-one 2 mm thick CT scans were obtained from the specimen. Scans were digitized using commercially available architecture and design software, and a virtual solid model was created. The model was then divided into 53 parts, each of which could be assigned its own set of elastic properties and then reassembled (Fig. 1A). Included among the 53 parts are 12 parts representing regions of trabecular bone (Fig. 1B).

Mesh Creation

During mesh creation, a complex object is modeled as a virtual mesh of many small simple elements. These elements generally take the form of bricks or tetrahedra. The elements are linked at their corner points, called nodes, and as the nodes are displaced, strain is generated in the elements. The finite-element model (FEM) of the macaque skull was constructed using 311,057 polyhedral elements containing between four and eight nodes each (Fig. 2). When constructing the FEM, the skull was aligned such that the occlusal plane was horizontal (i.e., in the X-Z plane). Note that the solid model used to create the FEM was so complex geometrically that mesh generation was extremely time-consuming. Thus, it was impractical to create multiple FEMs, each with different element densities (i.e., different numbers of elements). As a result, a convergence test was not performed.

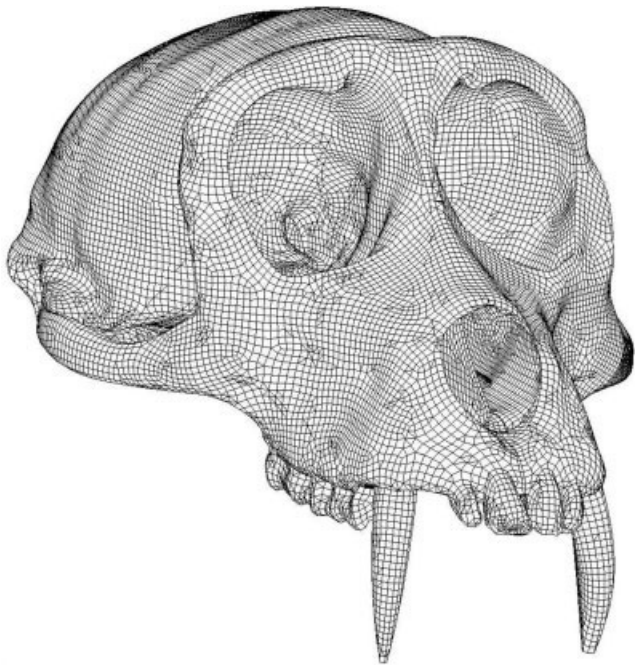

Fig. 2. Finite-element mesh consisting of 311,057 polyhedral elements.

Muscle Forces

Eight muscle forces were applied to the mesh, representing the right and left anterior temporalis, the superficial masseter, deep masster, and medial pterygoid. These muscles are principally responsible for jaw elevation during mastication. Muscle force magnitudes and orientations are summarized in Table 1. Force orientation was estimated by measuring the relative positions of muscle origins and insertions and by examining muscle maps based on dissections (Anton, 1993). Muscle force magnitude was estimated by combining data on muscle activity and physiological cross-sectional area. Within vertebrates, myofibrillar cross-sectional area is the closest correlate of force generating capacity (Murphy, 1998). Area and force are related such that 300 kiloNewtons are produced for every square meter of striated muscle (Murphy, 1998). Area data were obtained from Anton (1993). However, Anton (1993) did not collect data for the anterior temporalis in *M. fascicularis*. Thus, Anton's (1993) data for *M.*

TABLE 1. Muscle forces applied to finite-element model

Muscle	Magnitude in newtons	Orientation vector (x, y, z)[1]
Working-side superficial masseter	70.627	−0.2, −1, −0.2
Balancing-side superficial masseter	34.682	0.2, −1, −0.2
Working-side deep masseter	22.591	−0.6, −1, 0
Balancing-side deep masseter	8.214	0.6, −1, 0
Working-side medial pterygoid	34.794	0.75, −1, 0
Balancing-side medial pterygoid	6.904	−0.75, −1, 0
Working-side anterior temporalis	36.592	0.1, −1, −0.1
Balancing-side anterior temporalis	15.147	−0.1, −1, −0.1

[1]X-direction is positive to the model's left (working) side. Y-direction is positive superiorly. Z-direction is positive anteriorly.

fuscata were used instead for that muscle. *M. fuscata* is larger than *M. fascicularis*, and as a result the muscle force magnitudes employed in the model somewhat overestimate the forces actually generated by *M. fascicularis*.

Cross-sectional area measurements do not by themselves provide reliable estimates of muscle force because at any given moment, different muscles may have very different levels of activity. The relative force magnitudes exerted by each muscle at or near centric occlusion were calculated by assuming that force production is proportional to the magnitude of muscle activity as measured by the root mean square (r.m.s.) of electromyography (EMG) data collected during chewing experiments (Hylander and Johnson, 1989). The highest standardized r.m.s. EMG activity recorded from each electrode during an experiment is assigned a value equal to 100% of the cross-sectional area; when the muscle is acting at less than peak activity (e.g., at 50% of peak), then force is proportional to a corresponding percentage of cross-sectional area. EMG data gathered simultaneously from all eight muscles enable relative force magnitudes to be generated.

In FEA, loads are translated into strains instantaneously. When investigating chewing, a logical instant to model is the moment at which bite force is maximized. Bone strain magnitudes recorded from the lateral aspect of the mandibular corpus below M_{1-2} in macaques are highly correlated with the magnitude and timing of bite force during isometric biting on a force transducer ipsilateral to the strain gauge (Hylander, 1986), so the timing of peak bite force was estimated using the timing of peak strain in the mandibular corpus. Root mean square EMG activity in the masseter (Hylander and Johnson, 1989) and temporalis muscles precedes the force generated by those muscles by approximately 20 msec. Consequently, the muscle forces entered into the FEA were calculated from r.m.s. EMG activity 20 msec prior to the instant of peak corpus strain. In summary, muscle force magnitude is calculated as $F = (\text{cross-sectional area}) \times (300\ \text{kN/m}^2) \times (\%\ \text{of peak activity 20 msec prior to peak corpus strain})$.

Constraints

Three sets of constraints were applied to the model. Nodes at the right and left articular eminences and at the left M^1 were fixed in place. When muscle forces are applied to a model with these constraints, the model is pulled inferiorly onto the fixed points. Reaction forces are generated at each location, simulating the contact between the mandibular condyles and articular eminences, and between the teeth and a food item. Obviously, in life, the masticatory muscles act principally to move the mandible rather than the cranium. However, in a free-body diagram, pulling the skull down onto a bite point should produce forces in the face equivalent to those produced by pulling a mandible up onto a resistant food item, and then having the item contact a bite point on the upper tooth row. In either case, bite force is a reaction force at the bite point.

Elastic Properties

Elastic properties refer to the force-displacement relations of the substance being modeled. These relations are summarized by several variables, including the elastic modulus, the shear modulus, and Poisson's ratio. The elastic modulus (E) is defined as stress/strain (σ/ϵ) measured in simple extension or compression. It therefore describes numerically the stiffness of a material. For example, rubber will strain (deform) far more than steel under a given amount of stress and it has a correspondingly lower E. The shear modulus (G) is analogous to the elastic modulus in that it describes the stiffness of a material under shear. Poisson's ratio (v) is the lateral strain divided by axial strain, thus representing how much the sides of a material will contract as it is tensed (or, conversely, how the material will expand as it is compressed). E, G, and v are expressed along axes (or within planes defined by axes), and those axes have orientations that can be considered variables as well.

Bone presents a formidable modeling challenge for a number of reasons. First, the elastic properties of bone vary in different regions across the skull (Peterson and Dechow, 2003; and data not shown). For example, bone in the postorbital bar is 51% stiffer than bone in the adjacent supraorbital torus (as reflected by the elastic modulus in the axis of maximum stiffness). Moreover, bone is anisotropic, meaning that its elastic properties are not the same in all directions. More specifically, many regions of craniofacial bone are approximately orthotropic, meaning that bone exhibits three orthogonal material axes, each of which has its own set of properties. A further complication is that the orientation of the material axes may vary according to the shape of the bone. In most regions of cortical bone that have been investigated, including the facial skeleton, two of the three material axes are approximately parallel to the bone's surface, while the third axis is normal to the surface. Thus, if the surface of the bone is curved (as are many surfaces in the face), then the orientations of the material axes may vary with the curvature.

Although some finite-element analyses of osteological structures have used orthotropic elastic properties, the models used in those analyses have not been geometrically

TABLE 2. Elastic properties employed in analysis 3*

Region	Elastic modulus (E)[a,b]	Shear modulus (G)[a]	Poisson's ratio (v)
Premaxilla	18.5	5.6	0.21
P^3–M^1 alveolus	16.7	5.8	0.25
M^2–M^3 alveolus	20.6	6.4	0.27
Anterior palate	15.3	3.0	0.34
Posterior palate	18.8	2.6	0.32
Dorsal rostrum	19.9	6.9	0.22
Lateral rostrum	18.1	5.7	0.25
Root of zygoma	17.9	5.9	0.34
Anterior zygomatic arch	20.8	5.8	0.26
Posterior zygomatic arch	12.5	3.9	0.28
Medial orbital wall	14.6	5.6	0.36
Postorbital bar	19.8	6.3	0.27
Frontal torus	13.1	5.1	0.25
Glabella	14.4	4.4	0.27
Frontal squama	14.9	4.9	0.31
Neuro- and basicrania[c]	17.3	5.5	0.28

*From Wang and Dechow (unpublished).
[a]Values in GPa.
[b]Values represent axis of maximum stiffness.
[c]Average of values from all cranial regions.

complex (Korioth et al., 1992; Spears et al., 1993; Chen and Chen, 1998; Coleman et al., 2002; Snively and Russel, 2002). For example, the structures being modeled in those studies include long bones and mandibular corpora. In such cases, the major anatomical axes often coincide with material axes, making it relatively straightforward to model the material properties as orthotropic. However, more complex three-dimensional structures, such as the cranium, are often modeled isotropically (Witzel and Preuschoft, 1999; Rayfield et al., 2001; Cattaneo et al., 2003; Cruz et al., 2003). Whether modeled orthotropically or not, most FEA studies do not include information on the regional variation in material properties across the structure (but see Cattaneo et al., 2003).

Analyses

Given the complexity described above, it is not practical to model the elastic properties of bone with absolute precision. Rather, some simplifying assumptions about elastic properties are needed. However, those assumptions will not be useful if they cause a model to deform in an unrealistic fashion. In order to test the validity of possible modeling assumptions, four analyses were undertaken using four different approaches to modeling the elastic properties of cortical bone. In all analyses, trabecular bone in the supraorbital torus, postorbital bar, zygomatic body, and zygomatic arch was modeled isotropically (E = 0.64 GPa; G = 0.13 GPa; v = 0.28) (Ashman et al., 1989).

Analysis 1 (simple isotropy, human data). There are a number of approaches to modeling elastic properties. One approach is simply to obtain elastic properties data from the literature. This approach is advantageous in that it minimizes effort, but is disadvantageous in that one may not be able to obtain information about the species and/or skeletal element of interest. Moreover, such data may not provide information about regional variation or anisotropy in the bone being modeled. In analysis 1, cortical regions in the macaque skull model were assigned a single set of isotropic elastic properties (E = 18.0 GPa; G = 3.3 GPa; v = 0.3) derived from studies of human limb bones (Reilly and Burstein, 1975; Ashman et al., 1984; Currey, 2002).

Analyses 2–4. The alternative to employing published data is to collect elastic properties data on the skeletal element and species being modeled directly. An advantage of this approach is that elastic properties can be modeled with relative precision, but a drawback is that a considerable amount of time and effort must be invested into collecting the elastic properties data. Moreover, once the data are collected, one must then decide how those data will be used in the model. Analyses 2–4 reflect different ways of incorporating elastic properties data obtained from Wang and Dechow's unpublished examination of six adult *Macaca mulatta* skulls.

Analysis 2 (simple isotropy, macaque data). The simplest, but least precise method of incorporating Wang and Dechow's data is to assign the model a single set of isotropic elastic properties based on an average of values obtained from all parts of the skull (E = 17.3 GPa; G = 5.5 Gpa; v = 0.28).

Analysis 3 (regional isotropy, macaque data). A limitation of analysis 2 is that it does not incorporate regional variation in elastic properties. In analysis 3, each region of the skull was assigned its own set of isotropic elastic properties (Table 2). Note, however, that in this modeling approach, the boundaries between regions experience sudden shifts in elastic properties may not all be realistic.

Analysis 4 (regional orthotropy, macaque data). As in analysis 3, analysis 4 assigns each region its own set of elastic properties. Like analysis 3, there may be unrealistic shifts in elastic properties at boundaries between regions. Unlike analysis 3, analysis 4 models each region in the face orthotropically (the neuro- and basicrania were modeled isotropically as in analysis 3). Within each region, each of the three material axes is assigned a value

TABLE 3. Elastic properties employed in analysis 4*

Region	E_1[a,b]	E_2[a,b]	E_3[a,b]	G_{12}[a]	G_{13}[a]	G_{23}[a]	ν_{12}	ν_{13}	ν_{23}
Premaxilla	10.0	13.9	18.5	4.4	5.2	7.3	0.29	0.18	0.15
P^3–M^1 alveolus	9.9	12.1	16.7	4.3	5.8	7.4	0.33	0.24	0.17
M^2–M^3 alveolus	12.6	15.4	20.6	4.9	6.4	7.9	0.35	0.24	0.22
Anterior palate	7.5	8.8	15.3	2.6	2.8	3.6	0.41	0.36	0.26
Posterior palate	6.4	7.5	18.8	2.2	2.5	3.3	0.48	0.26	0.23
Dorsal rostrum	12.2	14.0	19.9	5.0	6.9	8.9	0.32	0.21	0.14
Lateral rostrum	11.5	14.4	18.1	4.7	5.3	7.3	0.37	0.24	0.15
Root of zygoma	8.9	10.9	17.9	3.7	5.3	8.6	0.53	0.30	0.18
Anterior zygomatic arch	8.6	12.4	20.8	4.2	4.6	8.6	0.39	0.28	0.22
Posterior zygomatic arch	8.2	10.0	12.5	3.1	3.8	4.9	0.34	0.27	0.24
Medial orbital wall	7.1	11.5	14.6	3.6	4.2	9.0	0.46	0.40	0.23
Postorbital bar	11.3	13.1	19.8	4.4	6.4	8.0	0.44	0.22	0.15
Frontal torus	10.2	11.2	13.1	4.3	5.1	6.0	0.32	0.24	0.19
Glabella	9.2	9.7	14.4	3.3	4.8	5.1	0.46	0.14	0.21
Frontal squama	7.9	11.0	14.9	3.4	4.3	7.1	0.49	0.27	0.18

*From Wang and Dechow (unpublished).
[a]Values in GPa.
[b]By convention, axis 3 is the axis of maximum stiffness. Axis 2 is perpendicular to axis 3 within the plane of the bone's surface. Axis 1 is perpendicular to the bone's surface. For each region, the orientations of these axes are derived from Wang and Dechow (data not shown).

for the elastic modulus, and each of the three planes defined by those axes receives values for the shear modulus and Poisson's ratio (Table 3). Moreover, the orientations of each of the axes are specified. Although the elastic properties employed in this analysis appear to be more precise than those employed in the other analyses, a potential problem with analysis 4 is that the material axes in each region receive only a single set of orientations. In regions with strongly curved surfaces, these orientations will not be accurate across an entire surface.

Evaluation of Analyses

In each analysis, strain data were recorded from 544 evenly spaced surface nodes. Comparison among the results of the four analyses is complicated by the fact that statistical tests (such as analysis of variance) are not obviously applicable. Statistical tests typically assess the probability that two or more groups of randomly sampled independent variates could have been drawn from a single statistical population. However, strain data derived from finite-element analyses are not independent because the degree of deformation recorded at a given node may influence deformation at adjacent nodes. Moreover, the strain data at the selected nodes are not randomly sampled. Rather, they are determined a priori by the boundary conditions (elastic properties, loads, constraints) of each analysis. Thus, the present study is not asking whether or not the four analyses are different from each other, because it is obvious that they are different. Rather, the present study is asking whether or not the magnitude of those differences warrants using more, or less, precise approaches to modeling elastic properties. This is a subjective question whose answer depends largely on the research goal of the investigator.

Results of the analyses were compared in three ways. First, a qualitative visual inspection of strain was performed. Next, the percentage difference in strain between models was calculated with respect to each of the 544 selected nodes. These differences were summarized by reporting the proportion of the nodes whose strain values differed in a given pair of analyses by more than 10%, 20%, 30%, 40%, and 50%. Finally, a validation study was performed on each analysis. Eight surface nodes were selected that represent locations from which in vivo experimental bone strain data have been collected in *M. fascicularis* and *M. mulatta* (Table 4). In each of the listed experiments, strain data were collected from multiple chews gathered from a single individual. Thus, within each experiment, geometry and elastic properties are held constant, but the muscle forces and the bite point may vary. Variation between experiments is presumably a consequence of all of the above variables. None of the experimental subjects were the subject of the FEM employed here, so there is no reason to expect that any one of the experiments is more relevant than any other for the purposes of model validation. Ideally, at any given location, the results of FEA would be considered realistic if FE strain values fell within the range of experimental values. However, ranges typically are not reported in the experimental studies employed here. Rather, those studies report a mean and standard deviation for each experiment. Those statistics were used to derive an approximate experimental range, calculated as the maximum range defined by the mean $\pm$ two standard deviations of each experiment. For example, five experiments have collected shear strain data from the balancing-side mid-zygomatic arch (Table 4). The upper and lower bounds of the approximate experimental range are provided by the means and standard deviations of experiments 2 and 9 from Hylander and Johnson (1997). The resulting range extends from 34 to 790 microstrain. This procedure is conservative in that it produces a wide envelope of strain values that can be considered realistic. Strain data from finite-element analyses that fall outside of the approximate experimental range can be safely considered unrealistic.

There are some caveats to the validation procedure. In particular, the model and experimental data differ in subtle ways that may affect validation. First, the published experimental data consist of peak strain values for a number of different regions on the facial skeleton. However,

TABLE 4. Validation data*

Region	Reference	Experiment	Mean maximum shear strain ± 2 standard deviations, in microstrain	Mean principal strain ratio ± 2 standard deviations
1, dorsal interorbital	Hylander et al. (1991)	5 A (W)	169 ± 94	2.1 ± 0.4
		5 A (B)	266 ± 82	2.3 ± 0.2
		6 (W)	185 ± 78	4.0 ± 0.4
		6 (B)	182 ± 68	4.0 ± 0.6
		2 A (W)	139 ± 110	1.8 ± 0.2
		2 A (B)	129 ± 42	1.7 ± 0.2
		2 B (W)	86 ± 38	2.4 ± 0.6
		5 B (W)	117 ± 56	3.1 ± 0.6
		5 C (W)	240 ± 116	2.6 ± 0.4
		5 C (B)	200 ± 84	2.1 ± 1.0
2, W dorsal orbital	Hylander et al. (1991)	5 A	100 ± 62	0.5 ± 0.2
		6	85 ± 44	0.7 ± 0.2
3, B dorsal orbital	Hylander et al. (1991)	5 A	147 ± 60	1.4 ± 0.2
		6	105 ± 29	1.4 ± 0.2
4, W infraorbital	Hylander et al. (1991)	2 C	325 ± 174	1.4[a]
		5 C	613 ± 256	1.1[a]
	Ross et al. (2002)	7	180 ± 128	0.1 ± 0.5[b]
5, B infraorbital	Hylander et al. (1991)		199 ± 144	2.2[a]
		5 C	295 ± 234	2.4[a]
	Ross et al. (2002)	7	192 ± 160	
6, W mid-zygomatic	Hylander et al. (1991)	2 A	661 ± 414	1.0[a]
		2 B	569 ± 244	0.9[a]
		5 B	250 ± 104	0.7[a]
	Hylander and Johnson (1997)	2	857 ± 360	0.6[a]
		5	614 ± 274	0.7[a]
		7	398 ± 204	0.7[a]
		9	391 ± 72	0.7[a]
7, B mid-zygomatic	Hylander et al. (1991)	2 A	352 ± 238	0.9[a]
	Hylander and Johnson (1997)	2	578 ± 212	0.5[a]
		5	440 ± 254	0.6[a]
		7	349 ± 262	0.6[a]
		9	202 ± 168	0.6[a]
8, W postorbital bar	Ross et al. (data not shown)	46	135 ± 113	1.0 ± 0.5[c]
		47	194 ± 197	
		48	142 ± 129	

*In all experiments, apple with skin is the food item being chewed. W, working-side; B, balancing-side. Note that in experimental studies, the orientation of maximum principal strain is measured quantitatively relative to the orientation of the strain gage on the skull, but the orientation of the gage is generally not reported quantitatively. Thus, validation of strain orientation relies substantially on visual inspection.

[a]Ratio of mean maximum and minimum principal strains.

[b]Data from this experiment were highly skewed, with most chews exhibiting high compression and low tension. However, the highest value observed in this experiment was 1.8.

[c]Data represent a combination of experiments 46 and 48.

not all regions experience peak strain at the same time during the chewing cycle, and thus peak strains from different regions are not precisely simultaneous. In contrast, the strains derived from FEA represent strains at a particular instant in time (i.e., the instant of peak corpus strain). Thus, there is an expectation that the strains at that moment of time in other regions may be at least slightly below peak. A second difference between the model and experimental data concerns dimensionality. Experimental strains are two-dimensional owing to the fact that strains can only be measured within the plane of the gauge. In contrast, model strains are three-dimensional, as are the strains actually experienced by the organism. Thus, experimental strains represent three-dimensional strains projected into two-dimensional space. If a given strain vector (e.g., maximum principal strain) has a strong directional component that is perpendicular to the gauge, then the gauge will underestimate the magnitude of the vector. Third, as mentioned, the specimen used to create the FEM is not one of the subjects of the in vivo experiments. Thus, the model and the experimental subjects undoubtedly differ with respect to craniofacial geometry, and some of those differences may impact strain patterns. Fourth, there is no information available as to whether the experimental subjects had patent or fused craniofacial sutures. Unfused sutures might be expected to dampen strain values, but sutures were not incorporated into the FEM. Finally, there is no information available as to which of the cheek teeth served as the bite point in any of the experimental chews. The position of the bite

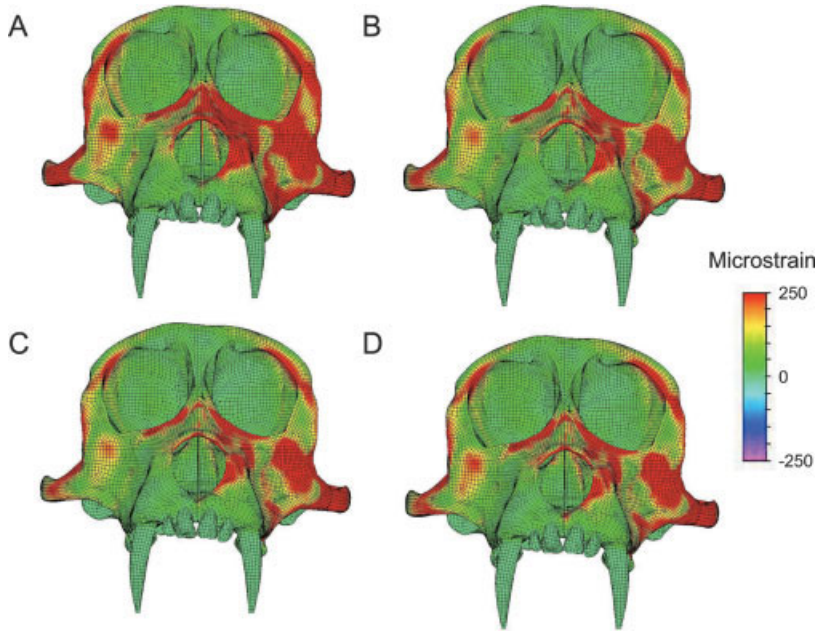

Fig. 3. Maximum principal strain in the finite-element model as induced by a left-side chew. Color mapping indicates the magnitude of strain. **A:** Analysis 1. **B:** Analysis 2. **C:** Analysis 3. **D:** Analysis 4. Note that strain concentrations are more extensive in A, reflecting the higher strain magnitudes in analysis 1.

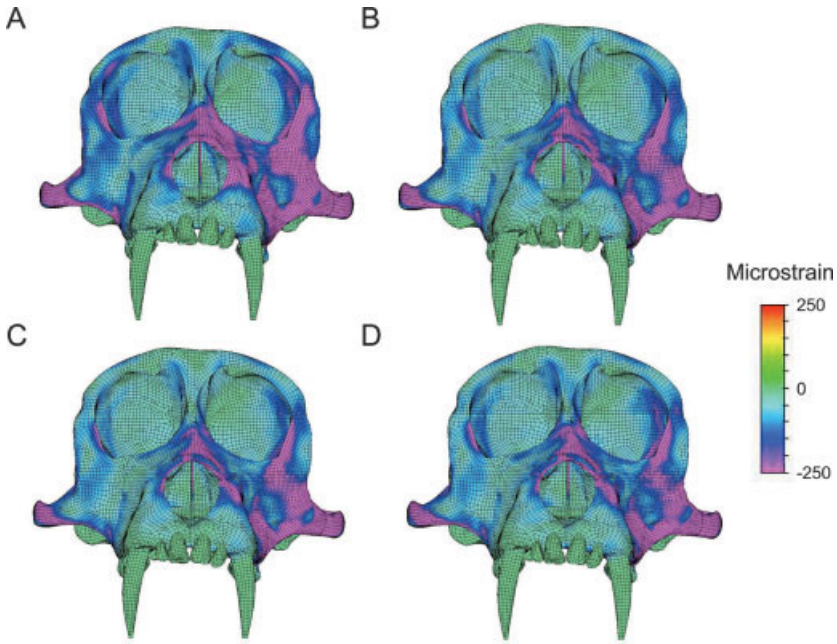

Fig. 4. Minimum principal strain in the finite-element model as induced by a left-side chew. Color mapping indicates the magnitude of strain. **A:** Analysis 1. **B:** Analysis 2. **C:** Analysis 3. **D:** Analysis 4. Note that strain concentrations are more extensive in A, reflecting the higher strain magnitudes in analysis 1.

point will obviously have an effect on bite force magnitude and on the bending moments experienced by various parts of the facial skeleton, and there is no reason to expect that the experimental subjects consistently used the same bite point.

RESULTS

Figures 3 and 4 illustrate the magnitudes of maximum and minimum principal strain, respectively, across the face in each of the four analyses. The spatial arrangement

TABLE 5. Comparisons between analyses (maximum shear strain)*

Comparison	Mean % difference (SD)	Percentage of nodes differing in shear strain by more than				
		10%	20%	30%	40%	50%
Analyses 1 vs. 2	39.0 (17.5)	97	86	67	48	25
Analyses 1 vs. 3	42.7 (22.4)	95	86	73	57	38
Analyses 1 vs. 4	35.9 (31.7)	86	73	57	45	35
Analyses 2 vs. 3	2.6 (9.0)	26	3	1	0	0
Analyses 2 vs. 4	−2.6 (17.1)	58	22	8	2	1
Analyses 3 vs. 4	−5.3 (13.1)	42	15	3	1	0

*In each analysis, strain is recorded at 544 surface nodes. In order to compare analyses, a percentage difference in strain is calculated for each node. For example, when comparing analyses 1 and 2, % difference = $(\text{strain}_{\text{analysis 1}} - \text{strain}_{\text{analysis 2}}) \times 100/\text{strain}_{\text{analysis 2}}$. Values greater than 10 or less than −10 indicate that the difference in strain at a given node is greater than 10%. This table indicates that in a comparison of analyses 1 and 2, 97% of the selected nodes differ in shear strain by more than 10%, 86% of nodes differ by more than 20%, and so on.

TABLE 6. Comparisons between analyses (ratio of maximum and minimum principal strains)*

Comparison	Mean % difference SD	Percentage of nodes differing in principal strain ratio by more than				
		10%	20%	30%	40%	50%
Analyses 1 vs. 2	0.9 (20.4)	62	33	14	5	0
Analyses 1 vs. 3	2.0 (26.3)	69	40	23	12	6
Analyses 1 vs. 4	5.5 (51.7)[a]	77	55	39	26	14
Analyses 2 vs. 3	0.3 (9.6)	23	4	1	1	0
Analyses 2 vs. 4	3.0 (47.8)[a]	63	32	16	7	5
Analyses 3 vs. 4	10 (35.8)[a]	56	23	9	5	4

*In each analysis, strain is recorded at 544 surface nodes. In order to compare analyses, a percentage difference in strain is calculated for each node. For example, when comparing analyses 1 and 2, % difference = $(\text{strain}_{\text{analysis 1}} - \text{strain}_{\text{analysis 2}}) \times 100/\text{strain}_{\text{analysis 2}}$. Values greater than 10 or less than −10 indicate that the difference in strain at a given node is greater than 10%. This table indicates that in a comparison of analyses 1 and 2, 62% of the selected nodes differ in principal strain ratio by more than 10%, 33% of nodes differ by more than 20%, and so on.
[a]High standard deviations in these comparisons are influenced by extremely high percentage differences (678–1,012%) at a few nodes.

of strain concentrations is broadly similar in all analyses. Visual inspection reveals few discernable differences between analyses 2–4 (Figs. 3B–D and 4B–D). Analysis 1 (Figs. 3A and 4A) differs from the other analyses in that its strain concentrations are more extensive, indicating that strain magnitudes are comparatively elevated.

Quantitative comparisons among analyses are presented in Tables 5 and 6. As a generalization, Analysis 1 is substantially different from analyses 2, 3, and 4, and analyses 2, 3, and 4 are only moderately different from each other. Whether or not those differences are meaningful depends on the degree of accuracy needed from the finite-element model. For example, if a given research question requires that the results of a model be accurate within 10%, then the differences between all of the models are arguably meaningful: in every comparison (Tables 5 and 6) strains in a sizeable proportion of nodes differ by more than that amount. However, if it is only necessary for a model to be accurate within 30%, then, with respect to maximum shear strain (Table 5), the differences between analyses 2, 3, and 4 are less meaningful than the differences between those analyses and analysis 1.

A factor complicating assessment of the analyses is the spatial patterning of strain differences. Depending on the analyses being compared, nodes in some regions can exhibit relatively high percentage differences in strain, while nodes in adjacent regions may exhibit more modest differences (Fig. 5). There is no obvious association between regions of high strain magnitudes and regions exhibiting high percentage differences (compare Figs. 3, 4, and 5). Rather, the spatial patterning reflects the regional patterning of elastic properties. For example, analysis 1 models elastic properties in a relatively coarse fashion, while analysis 4 models those properties more precisely. As a result, in some regions, analysis 1 will model bone as being stiffer than in analysis 4; in other regions, bone will be less stiff in analysis 1; in yet other regions, bone will be equally as stiff in the two analyses. Accordingly, the resulting strain differences (Fig. 5) will largely reflect this pattern. Thus, coarse approaches to modeling elastic properties might be adequate for certain regions of the model, but inadequate for other regions. However, there is no way of knowing which regions are suitable for a coarse approach until detailed data about elastic properties are collected, and the collection of such data defeats the purpose of that approach.

If a given research question dictates that approaches to modeling material properties might meaningfully impact results and interpretations, then which approach should be used? Validation studies, in which the results of the four finite-element analyses are compared to experimental data (Table 7), provide the best means for making an informed choice among approaches. With respect to maximum shear strain (Fig. 6), analysis 1 exhibited elevated

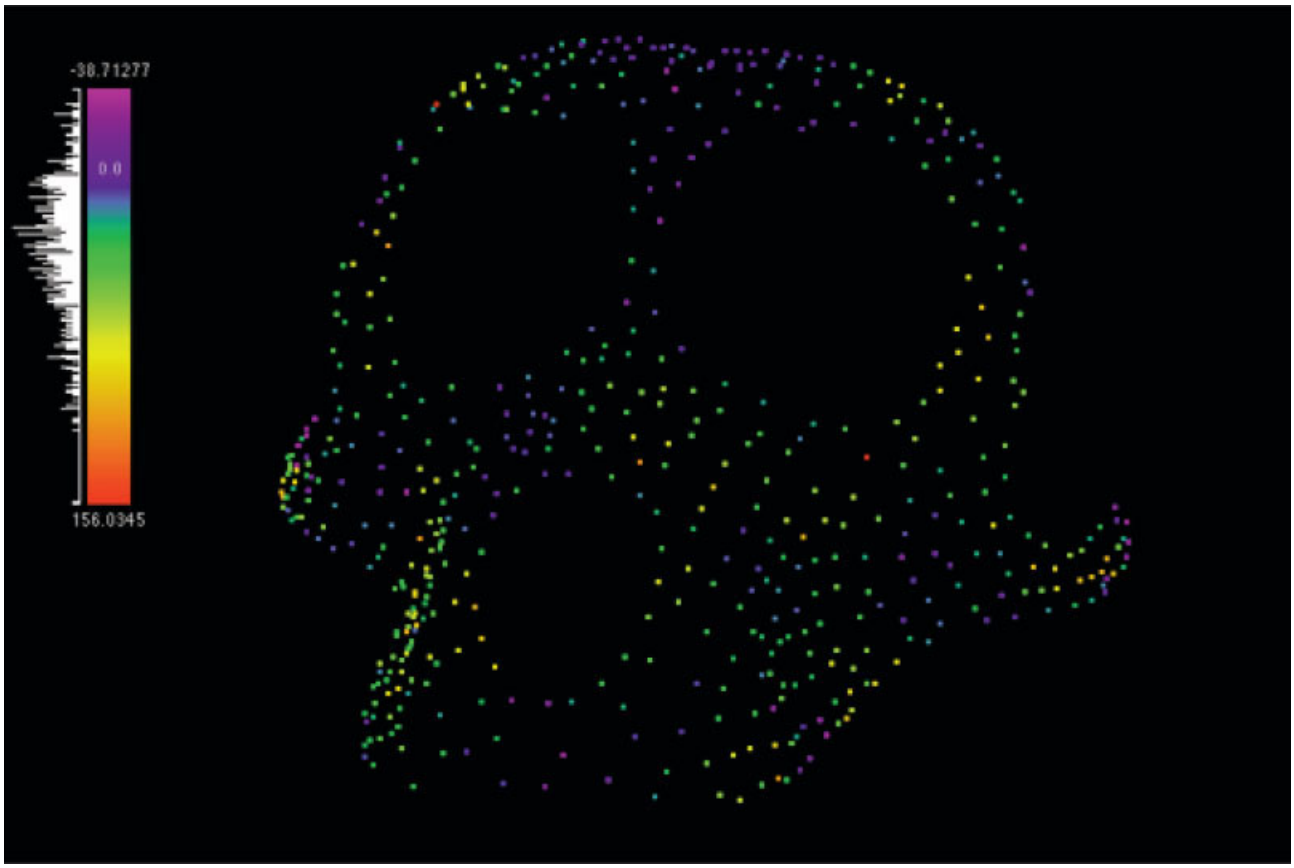

Fig. 5. Percentage difference in maximum shear strain between analyses 1 and 4. Each point represents a node on the surface of the finite-element model. Five hundred forty-four evenly spaced surface nodes are depicted, and the model is seen in a slightly oblique view. Percentage difference = $(\text{strain}_{\text{analysis 1}} - \text{strain}_{\text{analysis 2}}) \times 100/\text{strain}_{\text{analysis 2}}$. Positive values (green, yellow, red) indicate that shear strain is higher in analysis 1 than in analysis 2, while negative values (purple) indicate the reverse.

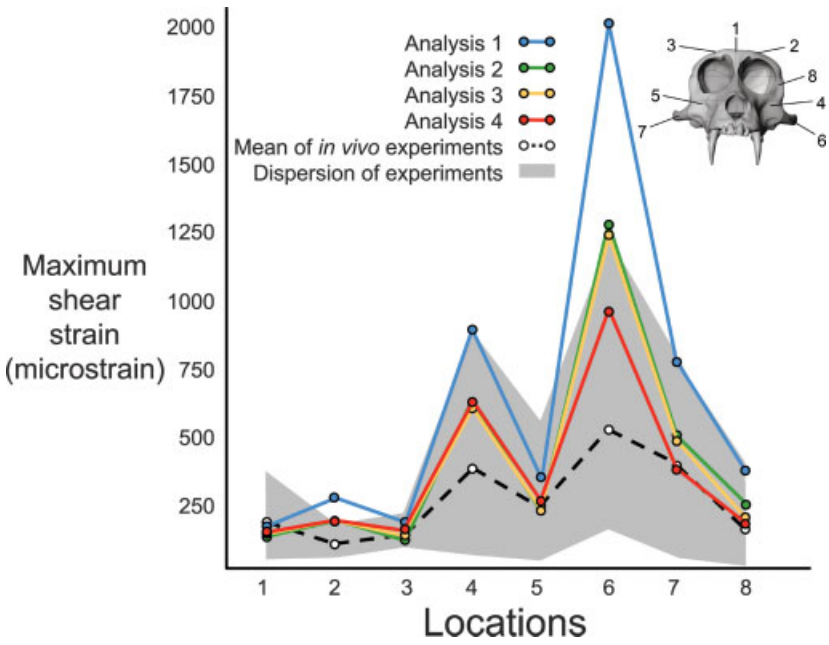

Fig. 6. Validation (maximum shear strain). Strains recorded in the four finite-element analyses are compared to strain data obtained from in vivo chewing experiments at eight locations on the skull. Locations labeled as in Hylander et al. (1991) and Ross and Hylander (1996): 1, dorsal interorbital; 2, working-side dorsal orbital; 3, balancing-side dorsal orbital; 4, working-side infraorbital; 5, balancing-side infraorbital; 6, working-side mid-zygomatic arch; 7, balancing-side mid-zygomatic arch; 8, working-side postorbital bar. The approximate range of experimental values is calculated as the maximum range defined by the mean $\pm$ two standard deviations of each experiment (Table 4). Thus, for location 4, the range is 52–869 microstrain, as indicated by experiment 7 of Ross et al. (2002) and experiment 5C of Hylander et al. (1991). Note that in many instances, the values for the analyses (particularly analyses 2 and 3) are extremely similar, causing the lines representing those analyses to overly each other virtually.

TABLE 7. Strain data from finite element analyses used for validation.

Region[a]	Analysis	Maximum shear strain, in microstrain	Principal strain ratio	Orientation of maximum principal strain (x, y, z)
1, dorsal interorbital	1	153	2.5	(0.97, 0.09, 0.23)
	2	122	2.9	(0.98, 0.04, 0.22)
	3	132	3.0	(0.97, 0.05, 0.22)
	4	139	4.4	(0.98, 0.07, 0.20)
2, W dorsal orbital	1	272	0.9	(0.71, 0.35, 0.61)
	2	190	0.7	(0.71, 0.38, 0.59)
	3	186	0.7	(0.72, 0.41, 0.56)
	4	184	0.6	(0.75, 0.36, 0.56)
3, B dorsal orbital	1	176	1.4	(0.88, −0.29, −0.37)
	2	128	1.3	(0.91, −0.20, −0.36)
	3	142	1.3	(0.91, −0.21, −0.37)
	4	159	1.3	(0.91, −0.25, −0.34)
4, W infraorbital	1	894	1.8	(0.73, 0.47, −0.50)
	2	680	1.8	(0.79, 0.40, −0.46)
	3	664	1.8	(0.81, 0.39, −0.45)
	4	683	2.0	(0.86, 0.26, −0.44)
5, B infraorbital	1	295	1.9	(0.73, −0.32, 0.61)
	2	219	2.7	(0.73, −0.37, 0.58)
	3	222	2.4	(0.78, −0.24, 0.58)
	4	269	2.3	(0.77, −0.10, 0.62)
6, W mid-zygomatic	1	2,010	0.8	(0.19, 0.77, −0.61)
	2	1,280	0.8	(0.22, 0.80, −0.56)
	3	1,230	0.8	(0.21, 0.79, −0.58)
	4	952	0.9	(0.18, 0.82, −0.54)
7, B mid-zygomatic	1	780	0.7	(0.96, 0.09, −0.26)
	2	500	0.7	(0.79, −0.56, 0.25)
	3	472	0.7	(0.76, −0.59, 0.27)
	4	368	0.7	(0.74, 0.49, −0.46)
8, W postorbital bar	1	379	1.0	(0.63, 0.73, 0.26)
	2	247	1.1	(0.57, 0.80, 0.19)
	3	199	1.0	(0.57, 0.80, 0.17)
	4	185	1.2	(0.58, 0.81, 0.10)

B, balancing-side; W, working-side.

strains that fell clearly outside the experimental dispersion with respect to two of eight locations on the skull. Shear strains at four other locations were near or just beyond the upper limits of the experimental dispersion. Analyses 2 and 3 exhibited very similar strain values and were just beyond the experimental dispersion with respect to two locations. Analysis 4 performed best insofar as its strain values tended to be closer to the experimental means than those of other analyses, and at only one location was shear strain just outside of the experimental dispersion.

With respect to principal strain ratio (Fig. 7), all analyses produced results that were broadly similar to experimental data. Although certain analyses fall beyond the dispersion of experimental data for some locations, those results are difficult to interpret because standard deviations are not published for those locations, and thus the experimental dispersion is not fully reported.

With respect to the orientation of maximum principal strain (Fig. 8), validation is complicated by the manner in which experimental strain orientations are reported. Strain orientations are measured quantitatively relative to the position of the strain gauge on the skull, but the position of the gauge is generally not reported quantitatively. Instead, gauge orientation is typically illustrated in a figure. Thus, validation based on strain orientation is largely qualitative. Given this caveat, analyses 3 and 4 performed best. In these analyses, strain orientations appeared to be within the experimental dispersion with respect to all but one region. Strain orientations in analyses 1 and 2 appeared to be outside the experimental dispersion with respect to three and two regions, respectively. None of the analyses produced realistic strain orientations in the working-side mid-zygomatic arch. The strain vectors produced by FEA instead resemble experimental strain vectors observed more posteriorly on the arch. Reanalysis of the FEM using quadratic elements (elements with mid-side nodes) in the zygomatic arches did not have a meaningful impact on strain orientations. A possible explanation is that the transition from the arch to the frontal process of the zygomatic is too abrupt in the model. In the actual specimen, the process grades into the arch, meaning that the anterior aspect of the arch should be inferosuperiorly thicker in the model. Insofar as a thicker anterior arch may influence how the arch bends, such morphology may have an effect on the orientation of strain in the middle of the arch.

To summarize the validation studies, all four analyses appear to be deforming in a broadly realistic fashion. However, on a finer scale, analysis 1 deforms in the least realistic fashion and is in some respects unrealistic. Analysis 4 deforms in the most realistic fashion. As a further generalization, the magnitude of difference exhibited between analyses tends to be less than or equal to the

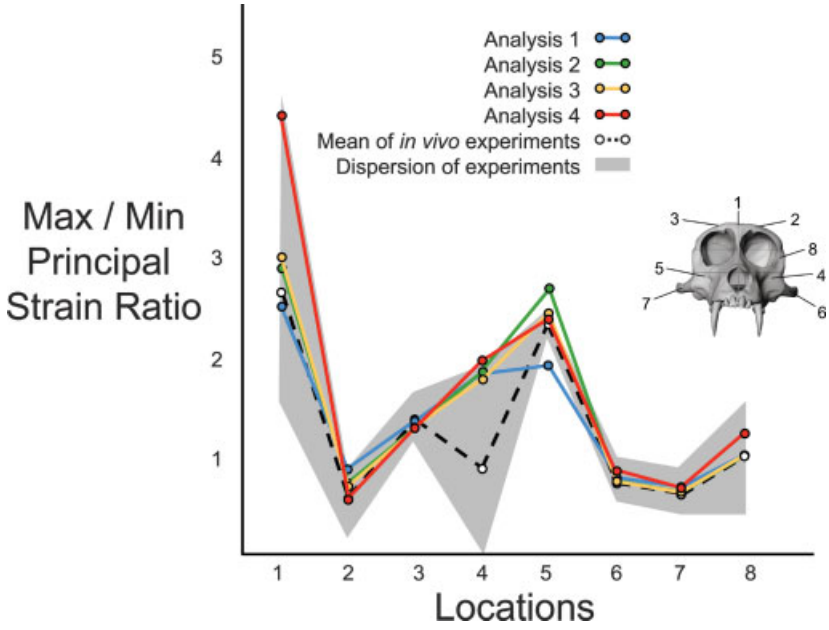

Fig. 7. Validation (principal strain ratio). Strains recorded in the four finite-element analyses are compared to strain data obtained from in vivo chewing experiments at eight locations on the skull. Locations and definitions as in Figure 5. Note that experimental standard deviations are not available for locations 4, 5, 6, and 7, and thus the ranges at those locations reflect only the range of experimental means.

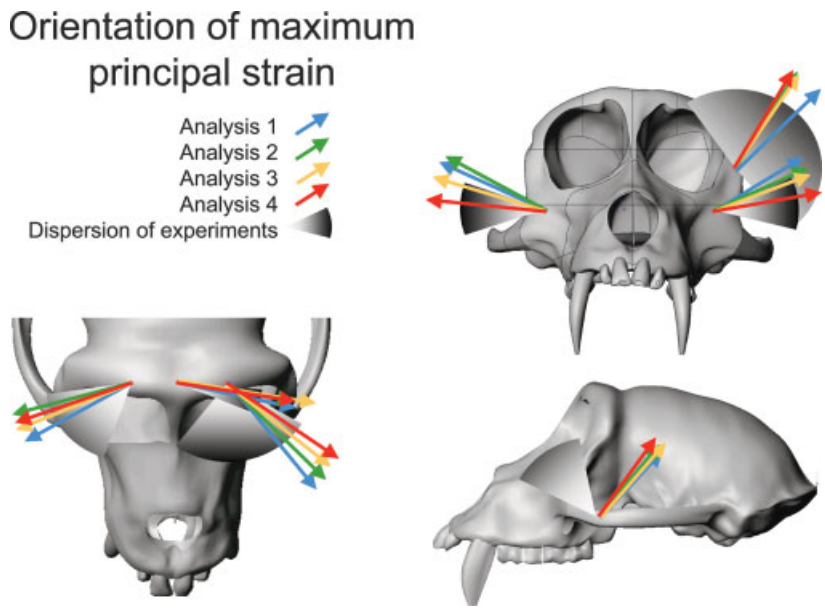

Fig. 8. Validation (orientation of maximum principal strain). Strains recorded in the four finite-element analyses are compared to strain data obtained from in vivo chewing experiments. Note that the orientations of strain gauges in the experiments have not been reported quantitatively (Hylander et al., 1991; Hylander and Johnson, 1997; Ross et al., 2002; and data not shown), and thus the dispersion of experimental values is only approximate.

magnitude of variability exhibited by the in vivo experimental data (Figs. 6, 7, and 8). Indeed, in many cases, the variation between analyses can be accommodated by variability within a single experiment (compare Tables 4 and 7). Thus, although some of the analyses exhibit strains that fall outside of the experimental dispersion, most of those strains might be best characterized as being moderately, as opposed to grossly, unrealistic.

DISCUSSION

The degree of precision needed when modeling elastic properties largely depends on the research questions to

which FEA is being applied. Figures 3 and 4 indicate that overall strain patterns are broadly similar in all of the analyses. Thus, if the goal of the analysis is to assess gross patterns of deformation qualitatively, then a relatively coarse approach to modeling elastic properties might be adequate. However, if the goal of FEA is to extract strain data for quantitative analysis, more precision may be required.

If primates are representative of other vertebrates, then one implication of the present study may be that having elastic properties data on the species and skeletal element being modeled is more important than how that data is used. The analysis based on data from human limb bones was notably different from all analyses based on macaque cranial data and performed least well in the validation studies. By comparison, differences between the three analyses that used data from the skulls of a closely allied macaque species were more modest, and they tended to perform better in the validation studies. The human limb data are similar to the macaque cranial data with respect to the elastic modulus and Poisson's ratio, so the differences between the models are presumably due principally to differences in shear modulus. With respect to most regions of the skull, macaque craniofacial bone is considerably stiffer in shear than is bone from the limbs of humans.

It is not surprising that in analyses of a macaque skull, FEA based on macaque cranial data performs better than FEA based on human limb data. However, the fact that the FEA based on human limb data deforms in a somewhat less realistic fashion means that researchers must be cautious when modeling elastic properties. From a modeling perspective, it would have been desirable if the FEA based on human limb data had performed equally well in validation, because that would have implied that the results of the FEA were robust to the modeling of elastic properties. Given that such a result was not observed, it is conceivable that a model that is geometrically precise could partially fail validation simply because of poor decisions about elastic properties. In order to minimize this possibility, modelers should work closely with bone biologists to obtain the needed elastic properties data. In the event that the species being modeled is known only from fossils (making it impossible to collect elastic properties data), then data should be obtained from the extant taxa that bracket the species phylogenetically (Witmer, 1995). Alternatively, histology or some other comparative criterion should be employed to select an appropriate extant analogue for the subject of the model (Rayfield et al., 2001).

If elastic properties data can be obtained for the species and skeletal element of interest, then it is desirable to incorporate information about regional variation and anisotropy. In the present study, the analysis that employed such information performed best in the validation study. A caveat is that if regions on the skull are defined too coarsely, such that the surfaces of the regions include substantial curvature, then information about anisotropy may introduce more error than accuracy into the analysis.

The present study also highlights the importance of validation in finite-element analysis. Without a comparison between the FEA and experimental data, it would not have been possible to determine that the realism of FEA is at least partially affected by approaches to modeling elastic properties. Similarly, without validation, any conclusions based on finite-element analysis should be interpreted cautiously. For example, if FEA produces results that might lead to an interpretation of function, behavior, or evolution, only validation can discount the alternative possibility that those results are a consequence of poor assumptions about geometry, loads, constraints, or elastic properties. Certainly, there will be circumstances in which validation data cannot be obtained, either because experiments cannot be performed on a given species, or because practical considerations preclude experimentation on a given skeletal element. In those instances, researchers should attempt to validate models of analogous organisms or skeletal elements so as to demonstrate, at a minimum, that the methods and assumptions used in their analyses are reliable.

As a generalization, biologists employ FEA because they are interested in the biomechanical consequences and correlates of skeletal form. Finite-element analysis is indeed a powerful tool for investigating such questions, but interpretations about form will not be possible if an analysis rests on imprecise assumptions about elastic properties, loads, or constraints. The present study suggests that for some research applications, it is important to obtain elastic properties data from the species and skeletal element being investigated. Failure to do so introduces a risk that the model will deform unrealistically and thus have limited utility for addressing biomechanical and evolutionary questions.

ACKNOWLEDGMENTS

The authors thank the International Congress of Vertebrate Morphology, *The Anatomical Record*, and the University of Chicago for sponsoring the symposium from which the present paper is derived. They also thank the participants of the symposium for many hours of insightful and enjoyable discussion. R. Thorington kindly allowed us access to specimens in his care at the National Museum of Natural History (NMNH) and B. Froelich allowed us to use the NMNH CT scanning equipment. In vivo macaque data were collected using funding from a National Science Foundation Physical Anthropology Grant (SBR 9706676; to C.F.R. and X. Chen). Finite-element analyses were supported by a National Science Foundation Physical Anthropology Grant (BCS 0240865; to D.S.S., P.C.D., B.G.R., C.F.R., and M.A.S.).

LITERATURE CITED

Anton SC. 1993. Internal masticatory muscle architecture in the Japanese macaque and its influence on bony morphology. Am J Phys Anthropol 16(Suppl):50.

Ashman RB, Cowin SC, Van Buskirk WC, Rice JC. 1984. A continuous wave technique for the measurement of the elastic properties of cortical bone. J Biomech 17:349–361.

Ashman RB, Rho JY, Turner CH. 1989. Anatomical variation of orthotropic elastic moduli of the proximal human tibia. J Biomech 22:895–900.

Borrazzo EC, Hylander WL, Rubin CT. 1994. Validation of a finite-element model of the functionally loaded zygomatic arch by in vivo strain gage data. Proc Am Soc Biomech 18:51–52.

Cattaneo PM, Dalstra M, Melsen B. 2003. The transfer of occlusal forces through the maxillary molars: a finite-element study. Am J Orthod Dentofacial Orthop 123:367–373.

Chen X, Chen H. 1998. The influence of alveolar structures on the torsional strain field in a gorilla corporeal cross-section. J Hum Evol 35:611–633.

Coleman JC, Hart RT, Owan I, Tankano Y, Burr DB. 2002. Characterization of dynamic three-dimensional strain fields in the canine radius. J Biomech 35:1677–1683.

Cook RD, Malkus DS, Plesha ME. 1989. Concepts and applications of finite-element analysis. New York: John Wiley and Sons.

Cruz M, Wassall T, Toledo EM, Barra LP, Lemonge AC. 2003. Three-dimensional finite-element stress analysis of a cuneiform-geometry implant. Int J Oral Maxillofac Implants 18:675–684.

Currey JD. 2002. Bones: structures and mechanics. Princeton, NJ: Princeton University Press.

Gross TS, Mcleod KJ, Rubin CT. 1992. Characterizing bone strain distributions in vivo using three triple rosette strain gages. J Biomech 25:1081–1087.

Huiskes R, Chao EYS. 1983. A survey of finite-element analysis in orthopedic biomechanics: the first decade. J Biomech 16:385–409.

Hylander WL. 1984. Stress and strain in the mandibular symphysis of primates: a test of competing hypotheses. Am J Phys Anthropol 64:1–46.

Hylander WL. 1986. In vivo bone strain as an indicator of masticatory bite force in *Macaca fascicularis*. Archs Oral Biol 31:149–157.

Hylander WL, Johnson KR. 1989. The relationship between masseter force and masseter electromyogram during masticcation in the monkey *Macac fascicularis*. Archs Oral Biol 34:713–722.

Hylander WL, Picq PG, Johnson KR. 1991. Masticatory-stress hypotheses and the supraorbital region of primates. Am J Phys Anthropol 86:1–36.

Hylander WL, Johnson KR. 1997. In vivo bone strain patterns in the zygomatic arch of macaques and the significance of these patterns for functional interpretations of craniodental form. Am J Phys Anthropol 102:203–232.

Korioth TWP, Romilly DP, Hannam AG. 1992. Three-dimensional finite-element stress analysis of the dentate human mandible. Am J Phys Anthropol 88:69–96.

Murphy RA. 1998. Skeletal muscle. In: RM Berne, MN Levy, editors. Physiology. St. Louis, MO: Mosby. p 294.

Peterson J, Dechow PC. 2003. Material properties of the human cranial vault and zygoma. Anat Rec 274A:785–797.

Rayfield EJ, Norman DB, Horner CC, Horner JR, Smith PM, Thomason JJ, Upchurch P. 2001. Cranial design and function in a large theropod dinosaur. Nature 409:1033–1037.

Reilly DT, Burstein AH. 1975. The elastic and ultimate properties of compact bone tissue. J Biomech 8:393–405.

Ross CF, Hylander WL. 1996. In vivo and in vitro bone strain in the owl monkey circumorbital region and the function of the postorbital septum. Am J Phys Anthropol 101:183–215.

Ross CF. 2001. In vivo function of the craniofacial haft: the interorbital "pillar." Am J Phys Anthropol 116:108–139.

Ross CF, Strait DS, Richmond BG, Spencer MA. 2002. In vivo bone strain and finite-element modeling of the anterior root of the zygoma in Macaca. Am J Phys Anthropol 34(Suppl):133.

Snively E, Russell A. 2002. The tyrannosaurid metatarsus: bone strain and inferred ligament function. Senckenbergiana Lethaea 82:35–42.

Spears IR, van Noort R, Crompton RH, Cardew GE, Howard IC. 1993. The effects of enamel anisotropy on the distribution of stress in a tooth. J Dent Res 72:1526–1531.

Witmer LM. 1995. The extant phylogenetic bracket and the importance of reconstructing soft tissues in fossils. In: Thomason JJ, editor. Functional morphology in vertebrate paleontology. Cambridge: Cambridge University Press. p 19–33.

Witzel U, Preuschoft H. 1999. The bony roof of the nose in humans and other primates. Zoologischer Anzeiger 238:103–115.